Journal of Materials and Environmental Sciences
ISSN : 2028-2508
CODEN : JMESCN

J. Mater. Environ. Sci., 2020, Volume 11, Issue 1, Page 57-68

http://www.jmaterenvironsci.com

Synthesis and characterization of $CuWO_4$ as nano-adsorbent for removal of Nile blue and its antimicrobial studies

B. Kavitha , R. Karthiga

P.G. & Research Department of Chemistry, C.P.A. College, Bodinayakanur-625513, Tamilnadu, India.

Received 29 May 2019,
Revised 26 Nov 2019,
Accepted 28 Nov 2019

Keywords
- ✓ $CuWO_4$,
- ✓ Adsorption,
- ✓ Kinetics,
- ✓ nile blue (NB),
- ✓ antimicrobial

kaviravee@gmail.com

Abstract

$CuWO_4$nanoparticles were prepared bysimple co-precipitation method and characterized using Fourier transform infrared spectroscopy (FT-IR), powder X-ray diffraction (XRD), scanning electron microscopy (SEM) and energy dispersive X-ray spectroscopy (EDS) techniques. The adsorption parameter of $CuWO_4$ was evaluated using nile blue (NB) as a model dye. Adsorption studies were conducted in a batch mode varying contact time, initial dye concentration and $CuWO_4$ dose. The equilibrium data were fitted to the Langmuir model and it follows the pseudo second order kinetic models. The antimicrobial activity was carried out against fungal strains (*candida albicans* and *Aspergillus niger*) and bacterial strains (*Staphylococcus aureus, Salmonella typhi* and *Klebsiella pneumoniae)*. $CuWO_4$ nanpoparticles showed excellent activity against *candida albicans* and *Staphylococcus aureus*.

1. Introduction

Nanostructured tungstate materials have aroused much interest because of their luminescent behavior, structural properties and potential applications. We are facing a great and growing concern for the environmental pollution problem and in particular for the progressive contamination of water reserves as a consequence of industrial development. Wastewaters containing dyes are difficult to remove because of their inert properties. Several techniques are available for the treatment of the dyes such as coagulation/flocculation, adsorption, ozonation, sodium hypochlorite treatment, photochemical decolourization, membrane separation process, electrochemical and aerobic and anaerobic microbial degradation, these methods are not very successfully due to suffering from many restrictions [1]. Among all of these methods, adsorption has been preferred due to its cheapness and the high quality of the treated effluents especially for well-designed sorption processes [2]. In particular, adsorption is recognized as an effective and economic method for the removal of pollutants from wastewaters [3]. Different adsorbents can be used for removal of dye, such as ceramics, waste materials, chitosan, agricultural waste, sepiolite, fly ash, hydrogels, perlite and activated carbon [4]. The efficiency and cost of these adsorbents vary from one material to another but high cost limits its commercial application. In recent years, extensive research has been undertaken to develop alternative and economic adsorbents [4]. The size, surface structure and interparticle interaction of nanomaterials concur on their unique properties and make their potential application in many areas.

Copper tungstate has attracted increasing interest from the research community because of its numerous possible applications. It has been suggested as a photoanode material candidate for photovoltaic electrochemical cells [5, 6]. In all-solid-state thin-film lithium batteries, which has $CuWO_4$ positive electrode shows a high-volume rate capacity in the first discharge and lack the unfavorable electrochemical degradation that is observed in liquid electrolyte systems.

Gupta et al synthesized guar gum–cerium (IV) tungstate to study its adsorption removal of methylene blue [7]. El-Kanash et al synthesized cerium tungstate to evaluate the inorganic exchange in sorption of cobalt and europium from aqueous solution [8].Wang et al reported adsorption capacity of Hexagonal tungsten trioxide nanorods on methylene blue [9]. Yourey et al studied electrochemical deposition and photoelectrochemistry of $CuWO_4$, a promising photoanode for water oxidation [10]. Pandey et al prepared $CuWO_4$ by Spray deposition process to study its photovoltaic electrochemical properties [11]. Ungelenk et al prepared a polyol-mediated low-temperature crystalline tungstate Nano particle [12]. Ruiz-Fuertes studied the growth, characterization, and high-pressure optical properties of $CuWO_4$ [13]. $CuWO_4$ have attracted much attention due to their interesting structural and photoluminescence properties. These materials have found applications in scintillation counters, lasers and optical fibers. $CuWO_4$ has also gained commercial interest in lasers and fluorescent lamps, while some are of special importance due to their electrical conductivity and magnetic properties. In addition, these materials also find applications as catalysts and humidity sensors [14].

In the present study a simple co-precipitation method was followed to prepare $CuWO_4$. The final adsorbent was characterized by Fourier transform infrared spectroscopy (FT-IR), powder X-ray diffraction (XRD), scanning electron microscopy (SEM) and energy dispersive X-ray spectroscopy (EDS) techniques. The adsorption behavior of $CuWO_4$ nanoparticles towards NB was investigated with respect to differential condition such as contact time, initial concentration and $CuWO_4$ dosage. The first report dealing with the application of $CuWO_4$ nanoparticles for separation and concentration of NB from large volume of water sample and its antimicrobial activity was reported here.

2. Materials and Method

Analytical-grade cupric chloride and sodium tungstate were used as received from Merck Company India. Nanosized powder of Copper tungstate were prepared by reacting aqueous solution of $CuCl_2.2H_2O$ (8.5 g) and $Na_2WO_4 \cdot 2H_2O$ (16.49 g) at room temperature at constant stirring. The formed blue precipitate was filtered and washed with distilled water a number of times and dried in an air oven at 100°C for 2 hours, then calcinated at 500°C for 2h to obtain $CuWO_4$ [15].

2.1. Characterization methods

X-ray diffraction spectrum was measured on a XPERT PRO X-RAY diffractometer with Cu Kα at 25°C to determine the crystalline structure. Surface structure was characterized by a Fourier-transform infra red (FT-IR) spectrophotometer (JASCO-FT-IR-460 plus). Absorption spectra were recorded using a JASCO V-530 UV–Vis spectrophotometer. The elemental analysis was studied by an energy dispersive X-ray spectroscopy (EDS) attached to the SEM. pH was monitored using EUTECH instrument pH meter.

2.2. Adsorption studies

All the batch adsorption experiments were carried out under dark condition at 30˚C. The variation of NB concentration versus time has been measured by UV-Visible spectrophotometer at 635 nm. For kinetics studies the initial dye concentration and dosage of the adsorbent were 10μM/L and 400 mg/L respectively. The adsorbed dye amount per unit mass of adsorbent (q_t) at any time was calculated from the following equation:

$$q_t = (C_o - C_t) \times V/W \quad \text{----------(1)}$$

Where C_o (g/L) and C_t (g/L) are the initial and equilibrium liquid-phases concentration of dyes respectively, V is the volume of the solution (L), and W is the weight of the $CuWO_4$ (g)used [16].

2.3. Assay for antimicrobial activity of $CuWO_4$ against microorganisms

The $CuWO_4$ nanoparticles dissolved in sterilized distilled water were tested for their antibacterial activity by the agar diffusion method against fungal strains (*candida albicans* and *Aspergillus niger*) and bacterial strains (*Staphylococcus aureus, Salmonella typhi* and *Klebsiella pneumoniae)*. These microbes were grown on liquid nutrient agar media for 24 h prior to the experiment, were seeded in agar plates by the pour plate technique. The

five test organisms were swapped over the nutrient agar medium and the disks containing $CuWO_4$ nanoparticles were kept over the medium using sterile forceps.The plates were incubated at 37°C for 24 h. The inhibition zone was measured in (mm) [17].

3. Results and discussion

3.1 Characterizations

3.1.1 XRD

Fig.1 shows the XRD pattern for $CuWO_4$ nanoparticles. All of the peakscan be indexed to the known anorthic structure of the $CuWO_4$ (JCPDS No 88-0269). A series of characteristic peaks at 19.0 (100), 24.0 (110), 25.9 (101), 28.7 (111), 30.1 (111), 31.6 (111), 32.1 (111), 35.6 (012), 36.8 (002), 39.8 (120) and 42.9 (102) was observed. The strong intensity and narrow width of $CuWO_4$ diffraction peaks indicate that the resulting products are of high crystallinity. The size of nanoparticles using XRD pattern can be estimated from scherrer equation and the average crystallite size for $CuWO_4$ was determined as 56.99 nm [18].

$$D = \frac{K\lambda}{\beta\cos\theta} \qquad (2)$$

Where, β is the full width half maximum of the most intense 2θ peak, K is the shape factor (0.90). θ and λ are the incident angle and wavelength of X-rays respectively.

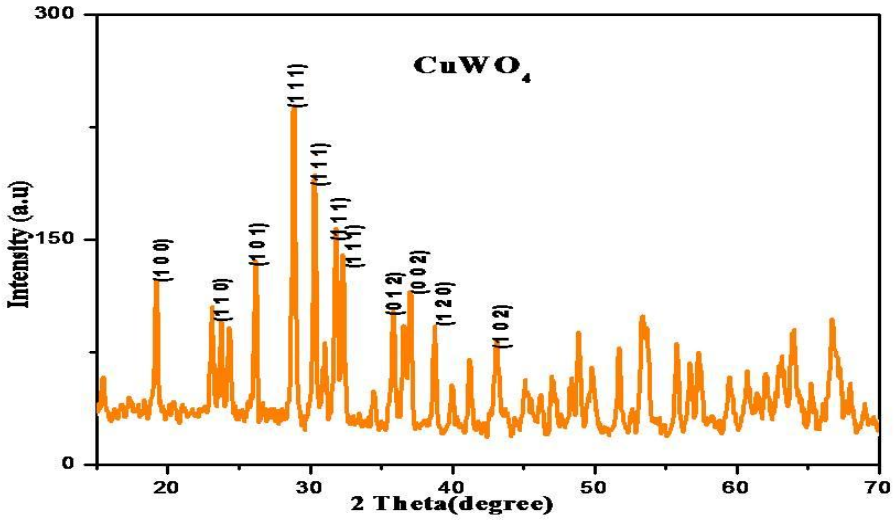

Fig.1 XRD for $CuWO_4$

3.1.2 FT-IR

FT-IR is recorded for quantities identification of surface functional groups. Fig.2 exhibits the FT-IR spectrum of $CuWO_4$ [19]. The absorption peak at 475cm^{-1}, 553cm^{-1} and 621cm^{-1} was due to the stretching of Cu-O. The band in the region 1063 cm^{-1} was due to W=O. The peak at 2362 cm^{-1} is due to that the spectrum was not recorded in situ and some absorption of H_2O from the ambient atmosphere has occurred [20].

3.1.3 SEM and EDX

Fig 5.(a) shows the SEM image of $CuWO_4$ nanoparticles calcinated at 500°C. The plate like structure is considered to have number of pores spaces where dyes can be adsorbed into these relatively large pores. To further demonstrate the formation of $CuWO_4$, their EDX spectrum was also analyzed. As shown shown in the figure 3(b), it was obvious that the element Cu, W and O wore co-present. The important peaks due to Cu, W, O are clearly distinct at 8.0 eV, 1.8 eV and 0.5 eV respectively and the result clearly indicating the formation of $CuWO_4$ nanoparticles.

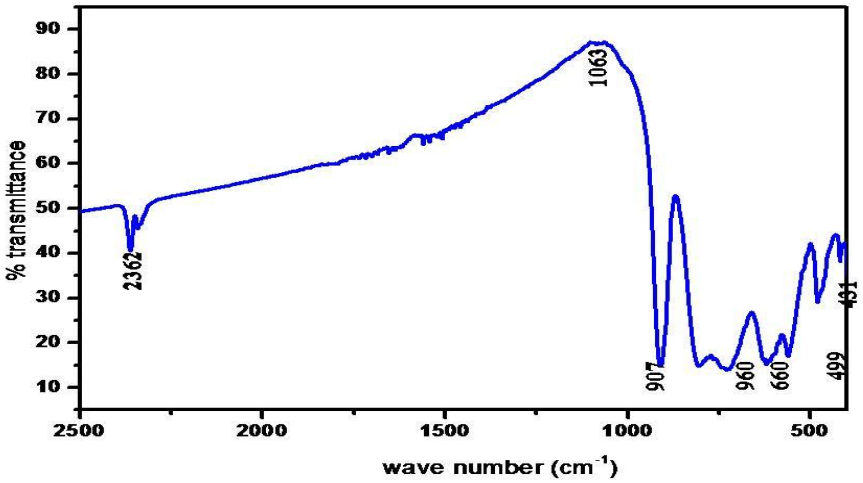

Fig.2 FT-IR spectrum of $CuWO_4$

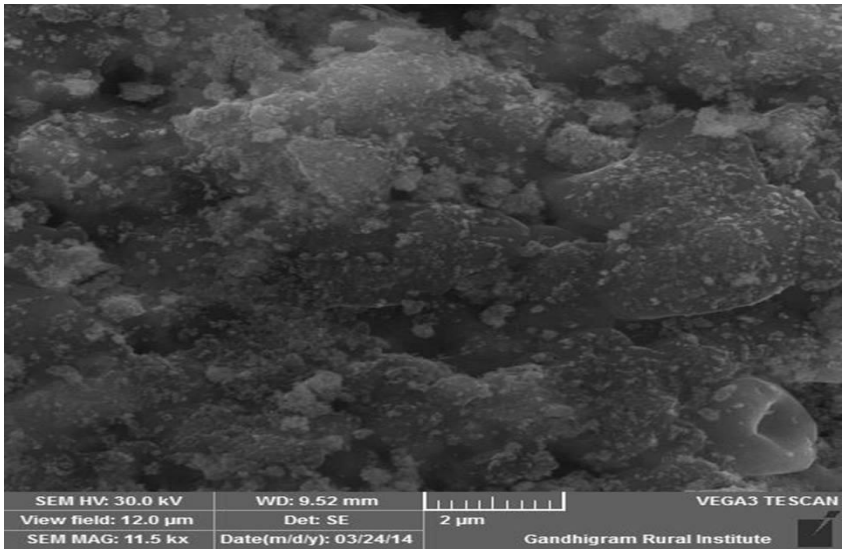

Fig.3.(a) SEM micrograph of $CuWO_4$

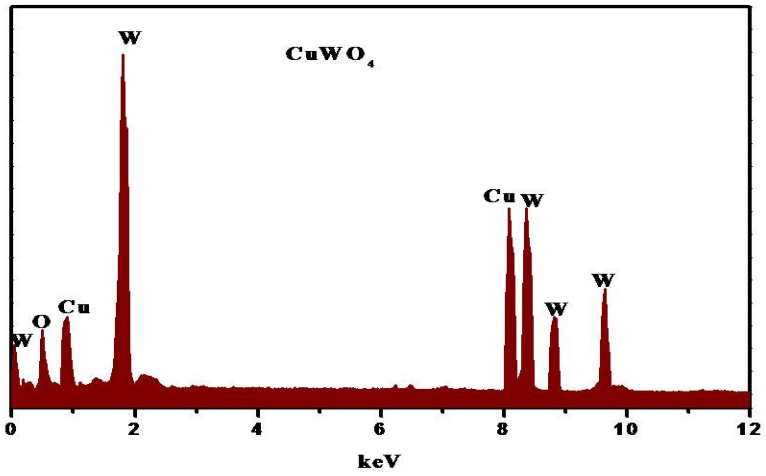

Fig.3.(b) EDX spectrum of $CuWO_4$

3.2.1. Effect of the dosage of $CuWO_4$ nanoparticles

The amount of absorbent is correlated with the amount of dye adsorbed. Thus, the effect of the amount of $CuWO_4$ was investigated. 100, 200, 300, 400, 500 and 600 mg/L of $CuWO_4$ nanoparticles were used and the results are shown in Fig.6. 400 mg of $CuWO_4$ could absorb the NB sufficiently and there is no change in the absorption on further increase of absorbent. Therefore, 400 mg/L of $CuWO_4$ is chosen as the optimum amount of absorbent in the following studies.

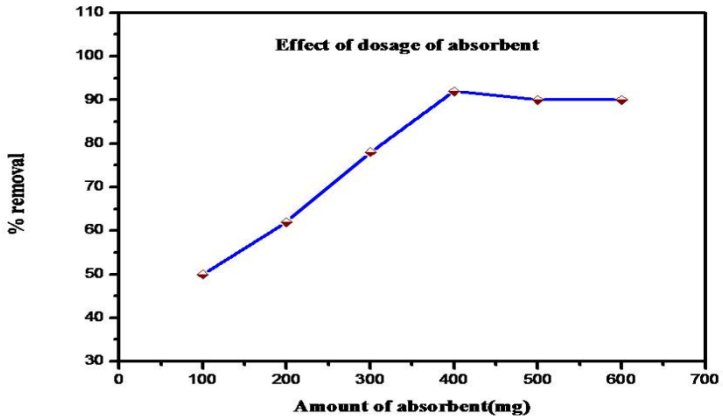

Fig.4 The effect of dosage of$CuWO_4$

3.2.2. Effect of contact time

The influence of contact time at fixed stirring percentage of absorption was investigated and the results are presented in the Fig.5. As it can be seen the amount and the percentage of NB removal increases with increasing contact time and about 50% removal of NB occurred within 30 min and the percentage of absorption increased slowly thereafter. The rapid adsorption at the initial contact time was due to the availability of more number of active sites on the adsorbent surface. The equilibrium was reached nearly at 180 min when the NB dye quantitatively adsorbed on the adsorbent surface.

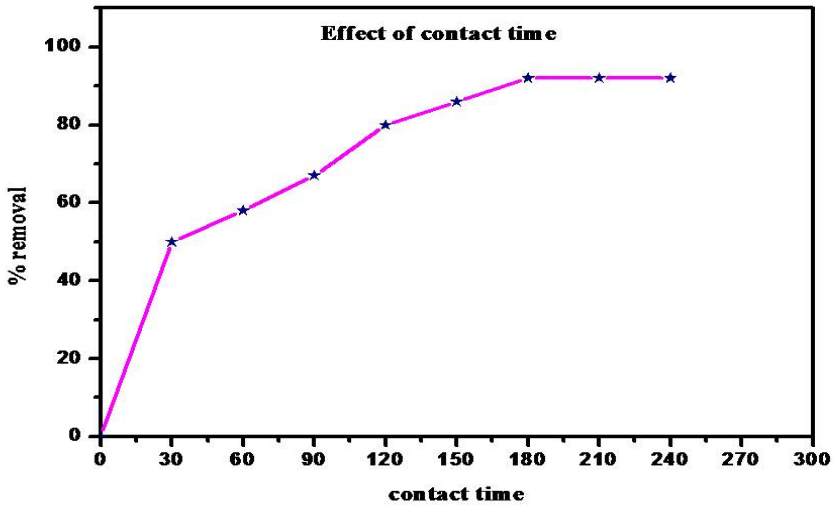

Fig.5 The effect of contact time on NB

3.2.3. Effect of initial concentration of nb dye

The effect of the initial concentration of NB dye on the adsorption efficiency of $CuWO_4$ nanoparticles was evaluated at different concentration of 10µM, 15µM, 20 µM and 25 µM. As Fig 6 depicts, one of the effective factors on the rate of dye uptake was the initial dye concentration of NB. It was seen that with the increase in the

initial concentration from 10 µM to 25 µM the percentage of dye removal was reduced from 92 to 60%. In addition, as the dye concentration increased, the number of available sites on the adsorbent surface decreased. For further analysis the initial concentration of NB was adjust to 10 µM.

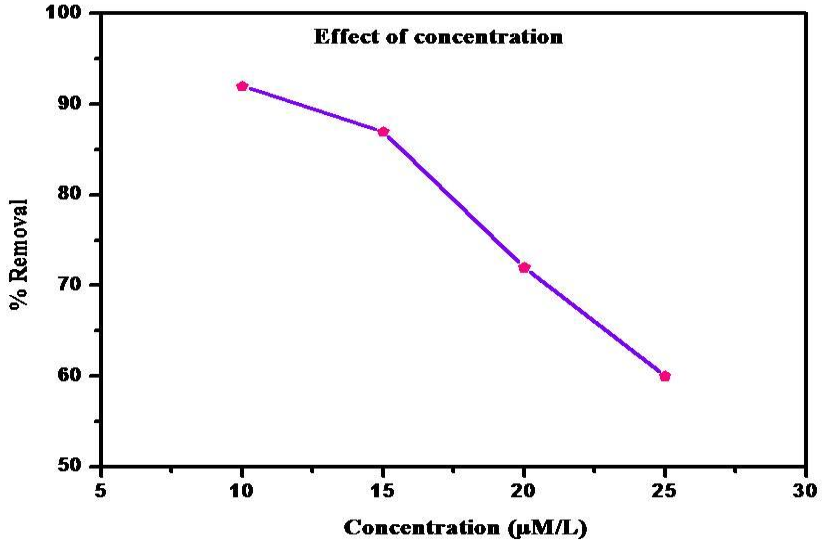

Fig 6 The effect of initial concentration on NB

3.3. Adsorption isotherm modeling

An adsorption isotherm describes the relationship between the dosage of adsorbate up taken by the adsorbent and the adsorbate concentration remaining in the solution [21]. The two important isotherms viz. Langmuir [22] and Freundlich[23] isotherms were investigated in this study.

The linearized form of Langumir adsorption model was given by the following equation.

$q_e = (K_L C_e / 1 + a_L C_e)$ ----------(3)

where, K_L is the Langmuir adsorption constant (L mg^{-1}) and Q_m is the maximum adsorption capacity (mg g^{-1}).

The linear form of Freundlichadsorption model was given by the following equation.

$\log q_e = 1/n \log C_e + \log K_f$ ----------(4)

where, value of K_F and 1/n was determined from the intercept and slope of linear plot of log q_e versus log C_e, respectively.

The Langmuir equation is valid for monolayer onto a completely homogenous surface with a finite number of identical sites with negligible interaction between adsorbed molecules. Fig. 7 shows the Langmuir (C_e/q_e Vs C_e) plot for the adsorption of NB. The isotherm of NB on $CuWO_4$ were found to be linear for the entire concentration range studies and the correlation coefficient were extremely high (R^2> 0.99) as shown in the Table 1.

Table . 1. Adsorption isotherm model parameters for adsorption of nileBlue(NB) on $CuWO_4$

dye	Langmuir			Freundlich		
	q_{max} (mg/g)	K_L (L/mg)	R^2	K_f (mg/g)	1/n	R^2
Nile blue(NB)	1.069	155.81	0.996	1.0439	0.001	0.001

The maximum adsorption capacity of the $CuWO_4$ in the Langmuir model was obtained as 1.069 mg/g which is considered as a favorable rate compared to Freudlich isotherm model. The Freudlich isotherm model [24] is derived by assuming a heterogeneous surface with a non-uniform distribution of adsorption over the surface. Fig.

8 shows the Freundlich (log q_eVs log C_e) plot for adsorption isotherm constant. The coefficient 1/n in the Freudlich model is a value between 0-1 which represents the adsorption intensity of the adsorbate to adsorbent. In the present work, the 1/n value revealed as 0.001.Hence, it can be concluded that Langmuir isotherm model is the best isotherm to predict the adsorption of nile blue dye over $CuWO_4$ adsorbent.

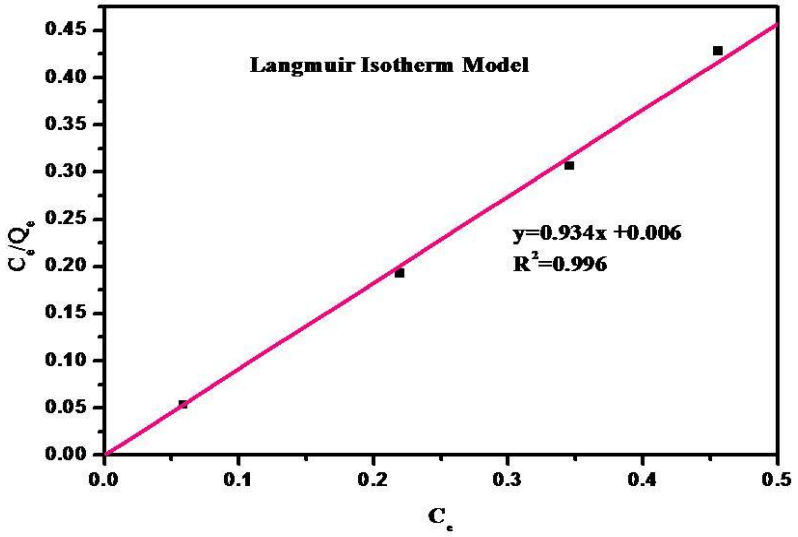

Fig. 7. Langmuir adsorption isotherm of NB

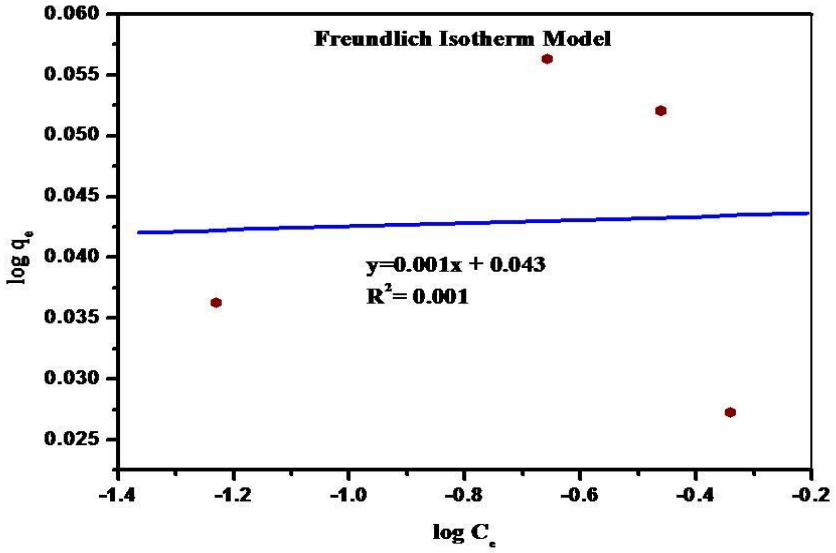

Fig.8 Freundlich adsorption isotherm of NB

3.4. Adsorption Kinetic modeling

In order to predict the mechanism of the present adsorption process and evaluate the performance of the adsorbent, three well known kinetic models were used to fit the experimental data: pseudo-first-order, pseudo-second-order kinetic models and the rate controlling step was determined by intra-particle diffusion model.

3.4.1. Pseudo-first-order model

Pseudo-first-order model was generally described by Lageregren [25] and might be represented by the following equation:

$\log(q_e-q) = \log q_e-(k_1/2.303)t$----------(5)

where q_e(mg/g) is the amount of dye adsorbed per unit weight of adsorbent at equilibrium i.e., adsorption capacity (mg/g), q(mg/g) is the amount of adsorbent adsorbed at any time t and k_1(min^{-1}) is the rate constant. The values of k_1 and q_e was calculated from the slope of the linear plot of $\log(q_e-q)$ versus t from equation 5.

3.4.2. Pseudo-second-order rate model

Pseudo-second-order rate model is given as follows:

$q/t=(1/K_2q^2_e) + (1/q_e)t$ ----------(6)

Where k_2 (g/mg min) is the rate constant. The values of k_2 and $q_e$can be determined from the plot of t/q against t from equation 6. Furthermore, the initial rate of adsorption (h) (mg/g min^{-1}), when $t\rightarrow0$, can also be calculated by using following formula:

$$h = K_2q^2_e$$ ----------(7)

Table .2 provides the pseudo-first-order rate constant k_1 and pseudo-second-order rate constant k_2, calculated equilibrium adsorption capacity q_e(theoretical) and experimental equilibrium adsorption capacity q_e(experimental) for initial dye concentration of 10µM. The q_e(theoretical) values calculated from pseudo-first-order kinetic model differed appreciably from the experimental values. However, in pseudo-second-order kinetic model the calculated q_e(theoretical) are very close to q_e(experimental) values for the dye. Further, the values of correlation coefficients (R^2) of pseudo-first-order model were slightly lesser than pseudo second- order model indicating that the pseudo-second-order model is better obeyed than pseudo-first-order model. The initial adsorption rate (h) calculated from pseudo-second-order rate equation for Nile blue was 0.075 mg/g min^{-1}.

Table.2 The kinetic parameters for adsorption of Nile blue on $CuWO_4$ nanoparticles

Dye	Experimental	Pseudo-first-order constants			Pseudo-second-order constants		
	q_e (mg/g)	q_e (mg/g)	k_1 (/min)	R^2	q_e (mg/g)	k_2 (g/mg/min)	R^2
Nile blue	1.0648	0.9371	0.0161	0.951	1.067	0.0659	0.977

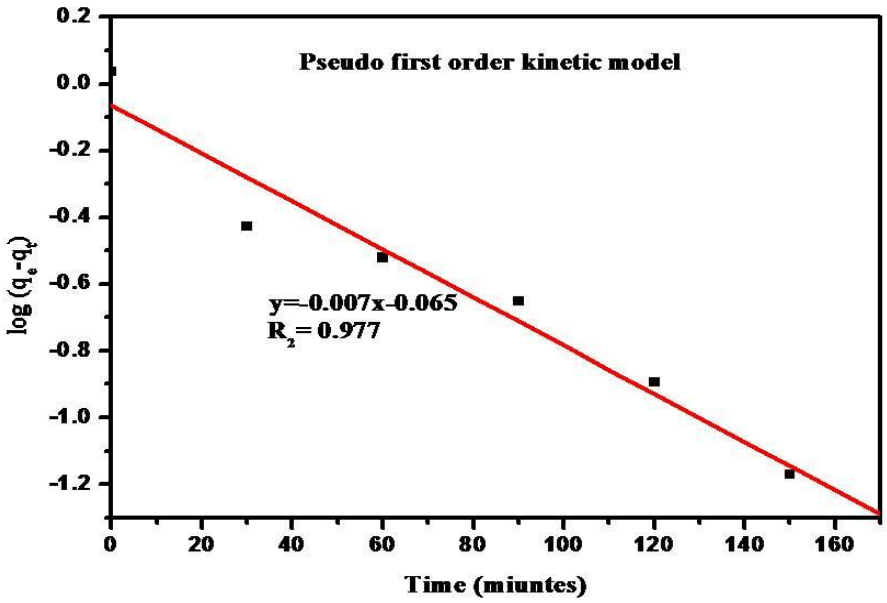

Fig.9 Pseudo first order model for nile blue

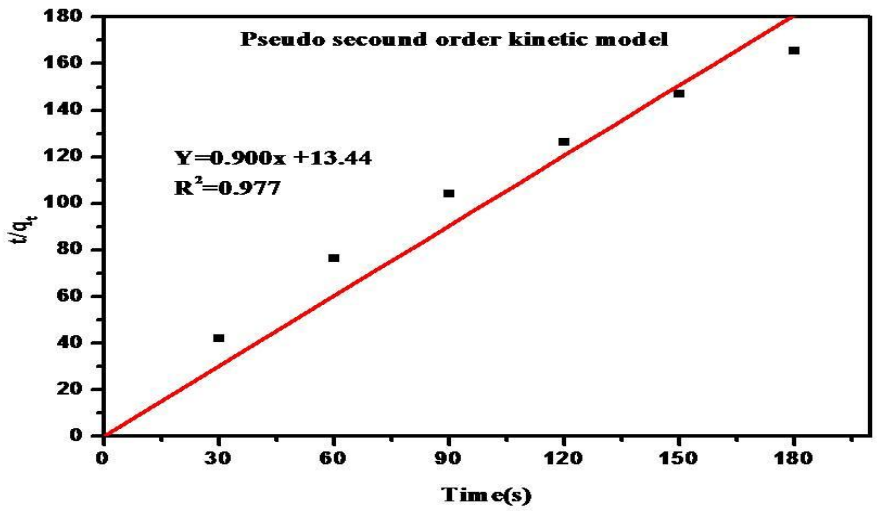

Fig.10 Pseudo second order model for nile blue

3.4.3. Intra-particle diffusion model (Waber–Morris model)

The overall reaction kinetics for the adsorption of Nile blue is a pseudo-second-order process. However, this could not highlight on the rate-limiting step. The rate-limiting step (slowest step of the reaction) may be either the boundary layer (film) or the intra-particle (pore) diffusion of solute on the solid surface from bulk of the solution in a batch process. The probability of the intraparticle diffusion was explored by using the following equation suggested by Weber and Morris [26, 27]:

$q_t = K_{id}t^{0.5} + C$----------(10)

whereq_t is adsorption capacity at any time t and k_{id} (mg/g $min^{0.5}$) isthe intra particle diffusion rate constant and C(mg/g) is a constant that gives an indication of the thickness of the boundary layer. Greater the value of C greater is the effect of boundary layer on adsorption process. If the rate limiting step be the intra-particle diffusion, the plot of q_t against the square root of time should be a straight line and pass through the origin. The deviation of the plot from the linearity indicates the rate-limiting step should be boundary layer (film) diffusion controlled. It can be seen from Fig.11.

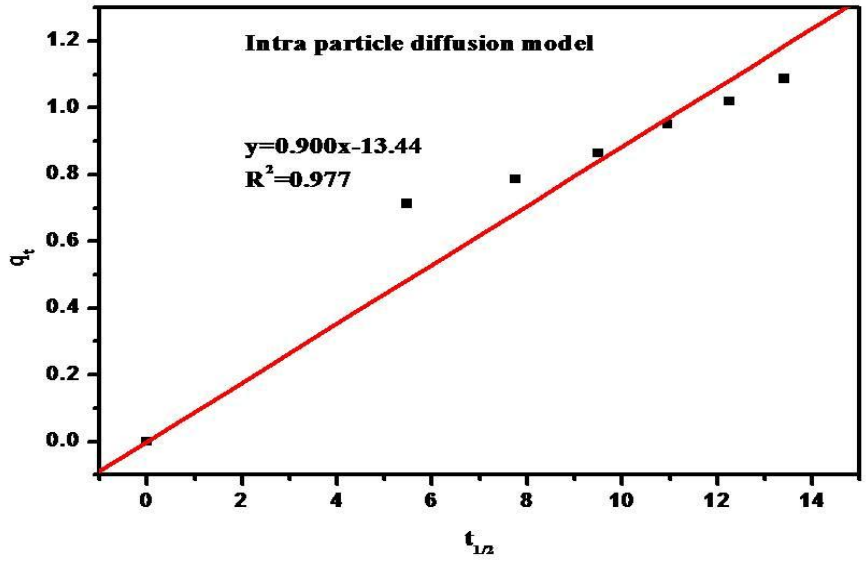

Fig.11 Intra-particle diffusion model for nile blue

The plots possess multi-linear portions; it indicates that the two or more steps influence the sorption process. It was found that three straight lines relate the points, the sharp first linear portion is due to the film diffusion and the second linear portion is due to the pore diffusion. Non-linearity of the plots had indicated the multi stage adsorption of Nile blue by $CuWO_4$ nanoparticles. The extrapolation of the first linear portion gives the intercept equal to the boundary layer thickness or film thickness.

3.4. Antimicrobial activity of $CuWO_4$

Antimicrobial activity of $CuWO_4$ was analyzed against fungal strains (*candida albicans* and *Aspergillus niger*) and bacterial strains (*Staphylococcus aureus, Salmonella typhi* and *Klebsiella pneumoniae)*. Figure12 and Table3 represent the results of antimicrobial activity of $CuWO_4$ for various microbes in a well diffusion assay. Amikacin was used as reference drug and Ketokonazole as control. The result revealed the potent antimicrobial activity of $CuWO_4$. The diameter of inhibition zone reflects magnitude of susceptibility of microbes. The strains susceptible to $CuWO_4$ exhibited larger zone of inhibition, where as resistant strains exhibit smaller zone of inhibition.

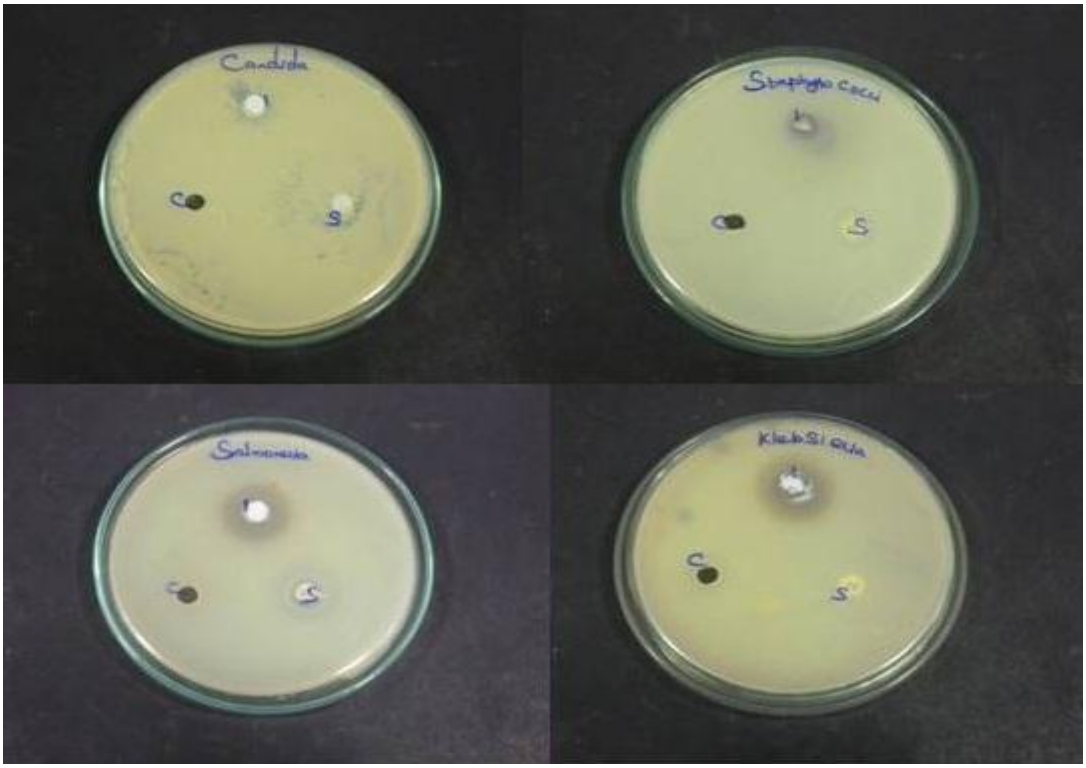

Fig.12 The photographs of antimicrobial activity of $CuWO_4$

Table.3 Anti-microbial activity of $CuWO_4$

Type of Pathogen	**Name of organism**	**Zone of inhibition in mm**		
		Control(Amikacin)	**Standard(**Ketokonazole**)**	**$CuWO_4$**
Bacterial strains	***Staphylococcus aureus***	**R**	**18**	**20**
	Salmonella typhi	**R**	**17**	**12**
	Klebsiella pneumoniae	**R**	**17**	**10**
Fungal strains	***Candida albicans***	**R**	**21**	**23**
	Aspergillusniger	**R**	**17**	**R**

According to zone of inhibition *candida albicans*(fungal strain) *and Staphylococcus aureus* (bacterial strain) exhibited the highest sensitivity toward $CuWO_4$. While *Klebsiella pneumonia, Salmonella typhi*(bacterial strain) showed the least sensitivity among the tested microbes. The antimicrobial activity of $CuWO_4$ depends on

several factors, including its degree of polymerization, molecular weight, nutrient composition, host, natural nutrient constituency, solvent, target microorganism, and physicochemical properties, and is inversely affected by pH [28].

Conclusion

$CuWO_4$ nanoparticles have been successfully synthesized by simple co-precipitation method. $CuWO_4$ nanoparticleswere characterized by FT-IR, XRD, SEM and EDX techniques. The removal efficiency and the adsorption capacity were found to be high for $CuWO_4$. The experimental data correlated reasonably well with Langmuir adsorption isotherm model and follows pseudo second order kinetics. Intra-particle diffusion model suggested that the initial adsorption rate controlled by the film diffusion, which followed by the pore diffusion. The strains susceptible to $CuWO_4$ exhibited large zone of inhibition against the pathogens like *candida albicans* and *Staphylococcus aureus*. Highest zone of inhibition was observed for *Staphylococcus aureus* of about 22 mm compared to other micro-organism.

References

1. R. Qadeer, Adsorption behavior of ruthenium ions on activated charcoal from nirtic acid medium, *Collids surf. A: Physicochem. Eng. Aspects* 293 (2007) 217-223. https://doi.org/10.1016/j.colsurfa.2006.07.035
2. M.T. Sulak, E. Demirbas, M.Kobya, Removal of Astrazon Yellow 7GL from aqueous solutions by adsorption onto wheat bran, *Bioresour. Technol.* 98 (2007) 2590-2598. https://doi.org/10.1016/j.biortech.2006.09.010
3. A.H. Chen, S.C. Liu, C.Y. Chen, C.Y. Chen, Comparative adsorption of Cu(II), Zn(II), and Pb(II) ions in aqueous solution on the crosslinked chitosan with epichlorohydrin, *J. Hazard. Mater.* 154 (2008) 184-191. https://doi.org/10.1016/j.jhazmat.2007.10.009
4. S.H. Jafari, S. Aziziana, B. Jalehb, Adsorption kinetics of methyl violet onto TiO_2 nanoparticles with different phases, Colloids. Surf. B: Physicochem. *Eng. Aspects.* 384 (2011) 618. https://doi.org/10.1016/j.colsurfa.2011.05.030
5. A.E.B. Lima , M.J.S. Costa, R.S. Santosb , N.C. Batista, L.S. Cavalcante, E. Longo , G.E. Luz Jr, Facile preparation of $CuWO_4$ porous films and their photoelectrochemical properties, Electrochimica Acta 256 (2017) 139–145. https://doi.org/10.1016/j.electacta.2017.10.010 0013-4686
6. W.J. Thomson, Introduction to Transport Phenomena, Prentice Hall PTR, NJ, USA, 2000.
7. V.K. Gupta, P. Deepak, S. Pardeep, K. Amit, B.S. Rathore, Adsorptional removal of methylene blue by guar gum–cerium (IV) tungstate hybrid cationic exchanger, Carbohydr 101 (2014) 684-691. https://doi.org/10.1016/j.carbpol.2013.09.092
8. A.M. Ei-Kamash, B. Ei-Gammal, A.A. Ei-Sayed, Preparation and evaluation of cerium(IV) tungstate powder as inorganic exchanger in sorption of cobalt and europium ions from aqueous solutions, J. Hazard. Mater. 141 (2007) 719-728. https://doi.org/10.1016/j.jhazmat.2006.07.041
9. F. Wang, C. Li, J.C. Yu, Hexagonal tungsten trioxide nanorods as a rapid adsorbent for methylene blue, Sep. Purif. Technol. 91 (2012) 103–107. https://doi.org/10.1016/j.seppur.2011.12.001
10. E. J. Yourey, M.B. Bartlett, Electrochemical deposition and photoelectrochemistry of $CuWO_4$ a promising photoanode for water oxidation, J. Mater. Chem., 21 (2011) 7651. https://doi.org/*10.1039/C1JM11259G*
11. P.K. Pandey, N.S. Bhave, R.B. Kharat. Spray deposition process of polycrystalline thin films of $CuWO_4$ and study on its photovoltaic electrochemical properties, *Mater. Lett.* 59 (2005) 3149. https://doi.org/10.1016/j.matlet.2005.05.018
12. J. Ungelenk, M. Speldrich, R. Dronskowski, C. Feldmann, Polyol-mediated low-temperature synthesis of crystalline tungstate nanoparticles MWO_4 (M = Mn, Fe, Co, Ni, Cu, Zn), *Solid State Sci.* 31 (2014) 62. http://dx.doi.org/10.1016/j.solidstatesciences.2014.02.020 1293-2558
13. J.R. Fuertes, D. Errandonea, A. Segura, F.J. Manjón, Z.h. Zhu, C.Y. Tu, Growth, characterization, and high-pressure optical studies of $CuWO_4$, High Pressure Research. 28 (2008) 565. https://doi.org/10.1080/08957950802446643

14. S.M. M Zawawi, R. Yahya, A. Hassan, H.N.M.E. Mahmud, M.N. Daud, Structural and optical characterization of metal tungstates (MWO4; M=Ni, Ba, Bi) synthesized by a sucrose-templated method, Chem. Cent. J. 7 (2013) 80. http://journal.chemistrycentral.com/content/7/1/80
15. S. Murni, M. Zawawi, R. Yahya, A. Hassan, H.N.M.E. Mahmud, N.D. Mohammad, Structural and optical characterization of metal tungstates (MWO_4; M=Ni, Ba, Bi) synthesized by a sucrose-templated method, Chem. Cent. J. 7 (2013) 80. https://doi.org/10.1186/1752-153X-7-80
16. Y.P. Chang, C.L. Ren, Q. Yang, Z.Y. Zhang, L.J. Dong, X.G. Chen, D.S. Xue, Preparation and characterization of hexadecyl functionalized magnetic silica nanoparticles and its application in Rhodamine 6G removal, Appl. Surf. Sci 257 (2011) 8610-8616. https://doi.org/10.1016/j.apsusc.2011.05.031
17. M.G. Nair, M. Nirmala, K. Rekha, A. Anukaliani, Structural, optical, photo catalytic and antibacterial activity of ZnO and Co doped ZnO nanoparticles, *Material Letter* 65 (2011) 1797. 10.1016/j.matlet.2011.03.079
18. J.I. Langford, A.J.C. Wilson, Scherrer after sixty years: A survey and some new results in the determination of crystallite size, *J. Appl. Cryst.* 11 (1978) 102-113. https://doi.org/10.1107/S0021889878012844
19. J. Jouhannaud, J. Rossignol, D. Stuerga, Rapid synthesis of tin (IV) oxide nanoparticles by microwave induced thermohydrolysis, J. Solid State Chem, 181 (2008) 1439. https://doi.org/10.1016/j.jssc.2008.02.040
20. K.N. Rao, A. Sridar, A.F. lee, S.J. Taveneer, N.A. Yong, K. Wilson, Zirconium phosphate supported tungsten oxide solid acid catalysts for the esterification of palmitic acid, Green chemistry 8 (2006) 790. https://doi.org/10.1039/B606088A
21. S. H. Kim, P.P. Choi, Enhanced Congo red dye removal from aqueous solutions using iron nanoparticles: adsorption, kinetics, and equilibrium studies, ***Dalton Trans.*** **46** (2017) 15470. https://doi.org/10.1039/C7DT02076G
22. A. Daneshyar, M. Ghaedi, M.M. Sabzehmeidani, H2S adsorption onto Cu-Zn–Ni nanoparticles loaded activated carbon and Ni-Co nanoparticles loaded γ-Al2O3: optimization and adsorption isotherms, J. Colloid Interface Sci. 490 (2017) 553–561. 10.1016/j.jcis.2016.11.068
23. Bazarafshan E. Efficiency of combined processes of coagulation and modified activated bentonite with sodium hydroxide as a biosorbent in the final treatment of leachate: kinetics and thermodynamics. J. Health Res. Commun. 3 (2017) 58. http://jhc.mazums.ac.ir/article-1-249
24. Yani Hua, Juan Xiao, Qinqin Zhang, Chang Cui, Chuan Wang, Facile synthesis of surface-functionalized magnetic nanocomposites for effectively selective adsorption of cationic dyes, Nanoscale Research Letters (2018) 13:99. https://doi.org/10.1186/s11671-018-2476-7
25. H. Rezaei, M. Haghshenasfard, A. Moheb, Optimization of dye adsorption using Fe_3O_4 nanoparticles encapsulated with alginate beads by Taguchi method, Adsorption Science & Technology, 2016, 1. https://doi.org/10.1177/0263617416667508
26. *M. N. Zafar, Q. Dar, F. Nawaz, M. N. Zafar, M. Iqba, M. F. Nazar,* Effective adsorptive removal of azo dyes over spherical ZnO nanoparticles,J. Mater. Res. Technol. 8(1) (2019) 713. https://doi.org/10.1016/j.jmrt.2018.06.002
27. C. S. Sundaram, N. Viswanathan, S. Meenakshi, Defluoridation chemistry of synthetic hydroxyapatite at nano scale: equilibrium and kinetic studies, *Journal of Hazardous Materials* 155 (2008) 206.
28. G. Sangeetha, S. Rajeshwari, R. Venckatesh, Green synthesized ZnO nanoparticles against bacterial and fungal pathogens, Progress in Natural Science: Materials International, 22 (2012) 693. https://doi.org/10.1016/j.pnsc.2012.11.015